Journal of Theoretical and Applied Information Technology

30th November 2023. Vol.101. No 22

ISSN: 1992-8645 www.jatit.org E-ISSN: 1817-3195

DENSE INCEPTION ATTENTION NEURAL NETWORK FOR ALZHEIMER'S DISEASE CLASSIFICATION USING MAGNETIC RESONANCE IMAGES

K. RANGA SWAMY[1], S. SENTHILKUMAR [2]

[1] Research scholar, Department of CSE, Presidency University, Bangalore

[2] Professor, Department of CSE, Presidency University, Bangalore

Email: rangaswamyphdcse@gmail.com[1], harisen1234@yahoo.co.in[2]

ABSTRACT

Alzheimer's disease (AD) is an irreversible disease and all currently available treatments may only delay its progress. Nonetheless, the diagnosis of AD, especially in the early stages, is important for preventing it from affecting daily life. Many current deep neural network models are designed to improve performance by deepening the number of network layers and widths for AD diagnosis using MRI images. It is characterized by both cognitive and functional impairment. However, as AD has an unclear pathological cause, it can be hard to diagnose with confidence. To address the above problems, this paper proposes a Dense Inception Attention Neural Network (DIAN-Net), which is a combination of the Dense module, skin connection, triple attention block, and the Inception attention module. The dense network uses depth separable convolution to remove the redundant operations of conventional convolution, constructs feature-separated distillation blocks as the basic feature extraction blocks of the network to extract multi-level depth feature information, and combines triple attention (TA) to enhance the feature mapping capability of the network and reduce model parameters and computation. The inception attention module is used to improve the receptive field and thus capture global feature information. The discriminative network makes the model more attentive to detailed image features and stabilizes the training process by taking into account the effects of different parts of the image. The experimental results show that the algorithm in this paper has a smaller number of parameters and shorter training time, and outperforms other methods in terms of subjective visualization and objective evaluation metrics on multiple benchmark datasets.

Keywords: *Alzheimer's Disease (AD), DCNN, Data Fusion, Dense Attention Network*

1. INTRODUCTION

Many image processing techniques are finding their way into medical image analysis as digital technology advances and the usage of imaging improves dramatically in healthcare and diagnostics. Researchers worldwide are putting massive efforts into enhancing automated diagnosis systems, making it one of the most active research areas. The fundamental reason behind making (CAD) based systems widely accessible and useful involves medical image segmentation as it has been used as a popular image processing technique to ease and automate medical imaging tasks[1-2]. During medical segmentation, the main objective is to extract the specific region of interest (ROI) from the medical images based on the intended application. After identifying the ROI, the primary focus is placed on investigating and analyzing the ROI obtained from medical image segmentation. This is particularly

useful in various medical applications, such as digital insertion of CAD-designed implants in a patient's body, simulating material properties, and many others. As a result, it assists doctors in analyzing and diagnosing the required region, such as infection, tumor, and so on[3-4]. The most prevalent type of dementia and a serious health concern in this day and age is Alzheimer's disease

[5]. By 2050, more than 1% of the world's population is expected to have AD or a similar condition, with a sizeable fraction of this group needing high-level care, according to Brookmeyer et al. [6]. Rare incidences of early-onset AD can afflict people between the ages of 45 and 64, while it typically affects people in their middle to late years [13]. Memory impairment [14], linguistic dysfunction [15], and a loss in cognition and judgment [16] are all signs of cognitive decline brought on by AD. Depending on the stage of disease progression, a person with symptoms may need some ongoing assistance with daily activities. The quality of life (QOL) of patients and their families is significantly impacted by these symptoms. The greater societal requirement for aged care greatly raises total socioeconomic pressure, according to studies on the expense of sickness for dementia and AD [17].People with AD may suffer from memory loss, progressive language impairment, a gradual decline in the ability to perform daily tasks, and abnormal changes in personality and behavior.

These symptoms can affect the person's life and severely reduce the life quality both for the person and their family. Moreover, AD is an irreversible disease and all current available treatments may only delay its progress. Nonetheless, the diagnosis of AD, especially in the early stages, is important, so that individuals and families can be aware and make adjustments to their lives as needed, but also since more precise diagnosis will be needed to develop new, potentially disease-modifying treatments [5-6]. The sample normal and AD images colle

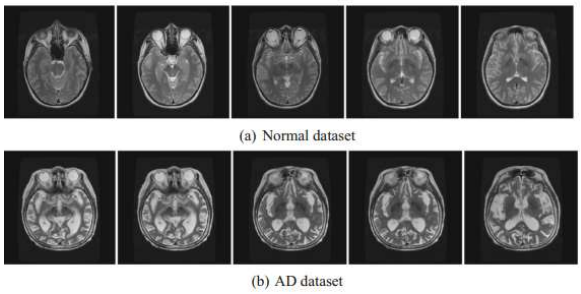

Fig. 1 Sample Test Images Considered From The Clinical Database

Many current deep neural network models are designed to improve performance by deepening the number of network layers and width, which undoubtedly increases memory consumption and training time [7]. With the increase of the number of convolutional layers, the network may suffer from the phenomena of gradient vanishing and gradient explosion, and also poor reconstruction results due to information loss. The super-resolution reconstruction network based on residual dense connectivity proposed by Zhang et al. [8] has deepened the implied layers to more than 100 layers, which achieves good performance but causes huge overhead, which makes the method unsuitable for practical applications.. Hui et al. [9] proposed a lightweight IDN (information distillation network), which uses a channel splitting method to reduce the network parameters by aggregating partially retained information with further extracted information, which can achieve better performance with a small number of parameters. However, the current lightweight super-resolution algorithms still have the problems of deep network layers, large number of parameters, and slow training speed, which not only tend to ignore the correlation between the intermediate layers and fail to make full use of the feature information of the images, but also fail to recover the texture details of the image, and obtain poor sensibility

Recently, machine learning technology has shown promising performance in AD incidence prediction with large-scale administrative health data (Park et al., 2020)[10]. A more objective approach to AD diagnosis is through biomarkers such as brain imaging (Wang et al., 2022; Khojaste-Sarakhsi et al., 2022)[11-12], and blood and cerebrospinal fluid examination. However, due to the unclear pathological cause, there is no uniform standard for AD diagnosis through biomarkers. Applying such tests for MCI is even less precise because of the heterogeneity of the syndrome of MCI. Consequently, with the development of artificial intelligence in the field of computer vision, computer-aided AD diagnosis, including prediction of AD and MCI, using medical images has become a research hotspot in recent years. Some recent studies have shown its capability in AD diagnosis with various modalities of radiography as input

including structural MRI (sMRI), functional MRI (fMRI) and positron emission tomography (PET).

2. RELATED WORK

Diagnostic criteria for AD and MCI are based on a variety of techniques. These techniques include cognitive evaluations like the Cambridge Cognitive Examination [19], Clinical Dementia Rating [18], and Mini-Mental State Examination [20]. These tests frequently include physical and neurological examinations and typically take the form of a series of questions. The diagnosis also takes into account medical history, family history, mental history, and a history of cognitive and behavioral abnormalities. Genetic predisposition is identified by sequencing for specific biomarkers, such as the APOE-e4 allele [21].

Neuroimaging is frequently used to examine different symptoms of brain alterations and rule out other possible explanations. To look for signs of brain atrophy, diffusion tensor imaging and structural magnetic resonance imaging are frequently used. Computed tomography (CT) in a variety of modalities is also used to diagnose AD and MCI. FDG-PET [22] examines the brain's glucose metabolism, while amyloid-PET is used to assess beta-amyloid levels during positron emission tomography (PET). Single-photon emission computed tomography (SPECT) [23] is unsuitable for clinical application and is likely to yield false-positive results. However, SPECT versions, such as the 99 mTc-HMPAO SPECT [24], may be employed in diagnosis. The nigrostriatal dopaminergic neurons can also be seen differently using FP-CIT SPECT [25]. Multimodality combinations are frequently employed in neuroimaging

Recent years have seen the implementation of new diagnostic CSF and blood plasma biomarkers that have been published in the literature. Amyloid-42, t-tau, and p-tau are the three primary biomarkers found in blood plasma and CSF. Neurofilament light protein (NFL), neuron-specific enolase (NSE), and HFABP are additional biomarkers. CSF biomarkers are increasingly important in some practices' criteria for diagnosing AD. However, only a post-mortem autopsy can provide the "ground truth" diagnosis of AD[26].

The NINCDS-ADRDA criteria were the accepted diagnostic standards prior to the twenty-first century. The International Working Group (IWG) revised these criteria in 2007 to include the necessity of at least one component among MRI, PET, and CSF biomarkers. In order to encompass both pre-dementia and dementia phases, a second modification was introduced in 2010. A third amendment was made to incorporate IWG-2, an unusual prodromal Alzheimer's disease that manifests as cognitive abnormalities other than memory impairment. The NIA-AA criteria, a different set of independent standards, were launched in 2011. Measures of brain amyloid, neuronal damage, and degeneration are some of these criteria. Each clinical stage, including pre-clinical, MCI, dementia, and post-mortem autopsy, was given its own set of criteria[27-28].

The established method in modern medical research involves extensive preprocessing, precise biomarker extraction, and statistical analysis. In their study of biomarkers derived from T1-weighted MRI scans of AD, MCI, and HC using voxel-based morphometry and parcellation methods, Risacher et al[29]. The study indicates statistical significance in a number of measurements, including entorhinal cortex thickness and hippocampal volume. This significance was further supported by Qiu et al. [30] who used large deformation diffeomorphic metric mapping (LDDMM) to examine regional volumetric changes. In order to find microRNA biomarkers in various stages of Alzheimer's disease, Guevremont et al. [31] concentrated on robustly detecting microRNAs in plasma and employed standardised analysis.

The established method in modern medical research involves extensive preprocessing, precise biomarker extraction, and statistical analysis. In their study of biomarkers derived from T1-weighted MRI scans of AD, MCI, and HC using voxel-based morphometry and parcellation methods, Risacher et al[29]. The study indicates statistical significance in a number of measurements, including entorhinal cortex thickness and hippocampal volume. This significance was further supported by Qiu et al. [32] who used large deformation diffeomorphic metric mapping (LDDMM) to examine regional volumetric changes. In order to find microRNA biomarkers in various

stages of Alzheimer's disease, Guevremont et al. [31] concentrated on robustly detecting microRNAs in plasma and employed standardised analysis.

Through a performance comparison between the Support Vector Machine (SVM) categorization of local grey matter volumes and human diagnosis by qualified radiologists, the work by Klöppel et al. [32] demonstrated the usefulness of using machine learning algorithms in detecting dementia. Using penalised regression with resampling, Janousova et al. [33] suggested looking for discriminative regions to help Gaussian kernel SVM classification. The study's regions were those previously identified by morphological investigations. These innovations sparked the creation of numerous machine-learning algorithms for the identification of AD and MCI.

Additionally, there has been a lot of interest in using deep learning (DL), a subset of machine learning, to study AD and associated disorders. Neural networks, which are general approximators based on backpropagation parameter training, are integrated with the two-step feature extraction and classification process through deep learning. [34]. Deep learning has significantly improved the analysis of medical data, such as those related to glioma , TB, and breast cancer. Deep learning use the hierarchical structure of neural networks for the automatic abstraction of several layers of features as opposed to manually creating features, models, and optimizers.

VGG16 is a convolutional neural network model used for image classification tasks. It was developed by researchers at the Visual Geometry Group (VGG) at the University of Oxford in 2014 and has 16 layers [18]. The VGG16 architecture is characterized by having very deep convolutional layers and small 3×3 convolution filters, which allows better feature extraction in high-resolution images. The model is trained on large and complex data sets, such as ImageNet, and has shown high performance in image classification tasks [19]. It is widely used in machine vision applications and has served as the basis for the development of other convolutional neural network models. [20]. The input of the first convolution layer (Conv2D) is an image of size 224X224. For all convolution layers, the convolution kernel is 3X3 in size. The layers are accompanied by Max-Pooling layers (MaxPool) that reduce the size of the filters during training. At the output of the convolution and pooling layers, there are three layers of fully connected neurons: Dense, Dense, and softmax to determine the image class.

3. DENSE INCEPTION ATTENTION NETWORK METHODOLOGY FOR AD DIAGNOSIS

Recently, many computer-vision works have been proposed for automatic classification of pathological images including traditional machine learning with hand-crafted features and burgeoning deep-learning methods. ResNet50 is a deep convolutional neural network model used for object recognition and image classification tasks. It was developed by Microsoft researchers in 2015 and has 50 layers. The name "ResNet" refers to the residual connections used in its architecture. These connections allow data to move directly from one layer to another, avoiding gradient fading problems and improving the ability of the network to learn and generalize from training data. ResNet50 is widely used in machine vision applications and has demonstrated high performance in image classification tasks on large and complex data sets . The notation $(k \times k, n)$ in each convolutional layer (conv) block denotes the size of the square matrix k and n channels, below each stage represents the repetition of each unit, the penultimate layer FC 1000 is the fully connected layer with a thousand neurons. Finally, $1 \times n$ represents the feature vector[35].

In this work, we will introduce our network, the Dense Inception Attention Network (DIAN-Net), it is a combination of the Dense module, skin connection, triple attention block, and the Inception attention module. The proposed network consists of major three parts: the base encoder-decoder framework, an improved Dense module, and an inception attention module. When solving the task of MRI image segmentation, a multi-scale input method is adopted. To ensure the model's ability to extract features, we use ResNet 50[29] as the

encoder. Feature information of the image passes into the image volume in the cumulative attention module.

3.1 Dense Attention Block

The conventional dual-convolution structure in U-Net has limited feature representation ability. In addition, due to the limited receptive field, there are still some shortcomings in multi-level context representation to affect the whole segmentation performance.

Conventional multi-scale feature representation is realized by convolutions with different kernel sizes. Nevertheless, large kernel sizes will introduce more computing costs to affect the inference efficiency of the segmentation network. Faced with the above issues, in order to fully extract image features and obtain multi-scale features, a dense attention block is proposed, and Fig.2 illustrates the specific network structure.

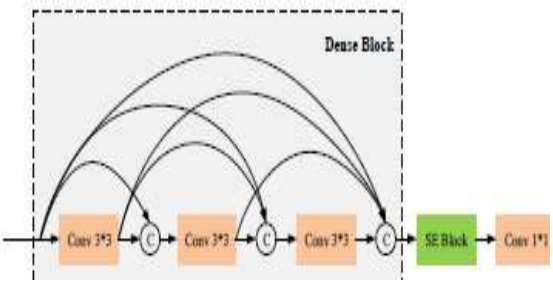

Fig. 2: Illustration Of Proposed Dense Attention Block.

For a dense attention block, it includes a dense convolution block and a channel attention block followed by a 1*1 convolution. To obtain multi-scale contexts, the dense convolution block is introduced to replace convolutions with large kernel sizes. Through the cascaded 3*3 convolution, it could acquire different receptive fields, such as 5*5 convolution, 7*7 convolution, etc. Eq.1 illustrates the process of dense block.

$$F_j = [F_{j-1} : F_{j-2}, \ldots, F_0] \quad (1)$$

where Fj indicates the input feature maps of j th convolution layer. Especially, each convolution layer follows a rectified linear unit (ReLU) function and a batch normalization (BN) layer.

Meanwhile, channel attention is adopted for channel calibration to obtain the channel weights. The squeeze-and- excitation block (SE) has been widely applied to different networks for channel calibration. It has shown a good performance optimization ability and could be easily to embed into any network. Here, it is introduced to make the proposed DIAN-Net focus on key channels. The output channel weights of the SE block is used to multiply with raw features by concatenation operation for suppressing irrelevant features and enhancing attention to the region of interest. Meanwhile, to cut the cost of computing, channel modification is also done using a 1*1 convolution.

3.2 Triple-attention Block

The AD regions are also against the class imbalance issue, which occupies a small-scale pixels. Meanwhile, the raw skip connections could not effectively process the local feature maps to bring the semantic gap issue. To effectively make full use of local feature maps and extract more useful features, a TA block is proposed to aggregate high-level features and low-level features for effective feature representation. Fig.3 illustrates the proposed TA block, and its mathematical description is given as Eq.2.

$$F_{att} = f_{CA}(f_{GA}(F_l, F_h)) + f_{PA}(f_{GA}(F_l, F_h)) \quad (2)$$

where Fh and Fl represent the high-level features by decoder and low-level features by encoder. fGA represents the global attention, and fCA and fP A represent the channel attention and position attention.

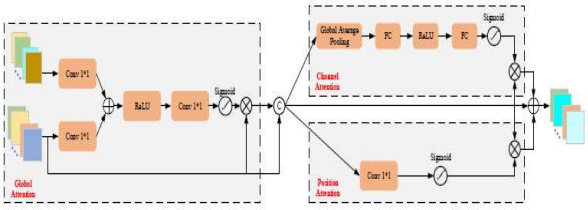

Fig. 3: Illustration Of TA Block.

For proposed TA block, the feature maps from encoder are firstly processed by global attention

block to extract the global contexts with the feature learning of feature maps from decoder (see Eq.3-4), and the irrelevant information in the feature map will be suppressed.

$$F_{gl} = \delta(Conv_{1*1}(ReLU(Conv_{1*1}(F_l) + Conv_{1*1}(F_h)))) \quad (3)$$

$$F_g = [F_{gl} : F_h] \quad (4)$$

where δ represents the sigmoid function, Conv1∗1 represents 1*1 convolution layer and : represents feature concatenation. After that, the output feature maps will be processed by

channel attention block and position attention block respectively to further enhance the attention of the segmentation network on the region of interest areas. Here, the SE block is also adopted to generate the channel attention features Fc. And the Fp could be acquired by multiplying the spatial weight with the input features to obtain position attention features, as Eq.5.

$$F_p = \delta(Conv_{1*1}(F_g)) \quad (5)$$

On the basis of channel attention block and position atten- tion block, the final attention feature maps could be obtained by element-wise summation of Fp and Fc.

Combined with the proposed TA block, the region of interest on feature maps could receive additional attention from the segmentation network, and it could fully extract the relationship between pixels to obtain more useful context features.

3.3 Dense-Inception Attention Module

In our Inception Attention module, various types of convolution kernels are put at the bottom of the model. These convolution kernels have different receptive fields and can extract features of different scales, and the transformation through convolution does not change the size of the original image. According to the Fourier Transformation theorem, such a convolution operation with padding can process meaning signals, superimpose these signals, and use the channel weight distribution mechanism to adjust parameters, so that the distribution of the obtained signals is more uniform, and there will be a lot of noise. The waveform is weakened, which can stabilize the training process of the model. The cooperation of Inception attention with the Dense module module is particularly critical. From the lattice classification results of graph convolution to the screening of multi-scale features, dense semantic information will be put into the entire attention feature extraction module.The proposed inception attention module is given in Figure 4.

Our Inception attention module is defined as follows: input global feature information X, after four convolution kernels, the output is output, as shown in Eqn 6:

$$X' = Conv3(X) + Conv5(X) + Conv1(X) + Conv7(X)$$

$$X'' = concat(Conv3(X), Conv5(X), Conv1(X), Conv7(X), X')$$

$$output = (W_1 \times sigmoid(Max(X'')) + W_2 \times sigmoid(Avg(X'')) + b) \times X'' \quad (6)$$

Among them, Conv1, Conv3, Conv5, and Conv7 represent 1×1, 3×3, 5×5, and 7×7 2D convolution kernels respectively, Max stands for max pooling, and Avg stands for avg pooling.
We demonstrate the importance of the combination of Inception structure and attention through ablation experiments.

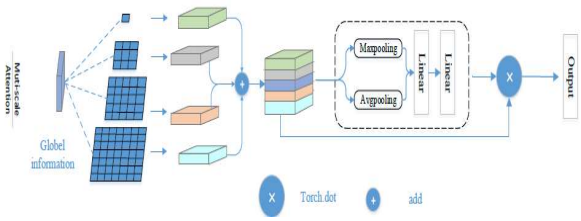

Figure 4. Inception Attention

3.4 Modified Skip Connections

The feature maps integrated via skip connections in the U-Net model's architecture contain a huge semantic gap since low-level features, which haven't been processed much, are combined with high-level features retrieved after numerous convolutions. Our proposed model incorporates skip pathways that serve as an alternative to skip connections.

Moreover, it has also been found that it effectively addresses the existing shortcomings due to the semantic level difference between low-level and high-level features. A sequence of skip blocks can be referred to as a skip path. A skip block comprises of a 3×3 convolution layer and a residual path convolution layer with a kernel size of 1×1. The obtained results are superior when a residual path is used instead of a convolution neural network. The lower-level features and higher-level features are concatenated in the UNet architecture. A huge semantic gap exists between the elements connected by the first skip connection link. The semantic gap between the second and third skip connections is smaller than the first, and so on. Considering this observation, the number of skip blocks in the skip path fluctuates. As a result, skip pathways 1, 2, 3, and 4 have a sequence of 4, 3, 2, and 1 skip blocks.

3.5 Loss Function

The loss function employed in the proposed medical image segmentation solution is the Jaccard Loss, which complements the Jaccard Coefficient by evaluating the dissimilarity between two samples. The Jaccard Coefficient is subtracted from 1 to get the Jaccard Loss. The Jaccard Index is computed by dividing the intersection size by the union size. The formula for Jaccard Coefficient has been given in Equation (**7**).

$$Jaccard\ Index = \frac{A \cap B}{A \cup B} = \frac{A \cap B}{A + B - A \cap B} \quad (7)$$

4. EXPERIMENTAL RESULTS

Cross-validation and the train/test set are two common techniques for evaluating the performance of a machine learning model. Both methods are used to assess a model's ability to generalize to unseen data, but they differ in the way the data is partitioned for evaluation. Cross-validation is a method that involves dividing the data set into k folds. The model is trained k times, each time using k-1 folds for training and the remaining fold for evaluation. Performance scores are calculated for each fold and averaged to get an overall measure of model performance. Cross-validation helps to reduce model evaluation scarcity and to obtain a more accurate estimate of model performance. The training/test set, on the other hand, involves dividing the data set into two exclusive sets: a training set and a test set. The model is trained on the training set and evaluated on the test set. The performance score is calculated based on the model's ability to generalize data not seen in the test set. In general, cross-validation is used when you have a limited data set and you want a more accurate estimate of the model performance, while a train/test set is a faster and easier technique used when you have a large data set, and a rapid evaluation of the model is desired.

4.1 Data set:

In real-world scenarios, the amount of medical imaging data available is limited. Therefore, it demands applying robust data augmentation techniques to increase the data size. For data augmentation, we employed the basic procedures where the images were horizontally flipped and rotated at a random angle of 40◦ clockwise and 40◦ anti-clockwise. After following these augmentation procedures, the number of images available in the dataset has approximately doubled. We have shown the samples of images and their respective masks obtained after applying augmentation techniques. The dataset used in this study is from the Alzheimer's Disease Neuroimaging Initiative (ADNI), which is openly available online at http://adni.loni.usc.edu. The ADNI wants to create more accurate and sensitive ways to identify Alzheimer's disease in its early stages with the aid of biomarkers. For this investigation, we used 694 structural MRI images, of which 198 were classified at baseline as AD, 230 as NC, 166 as pMCI, and 101 as MCI. The 166 pMCI individuals were initially diagnosed with MCI at baseline, however, it was later found that they had changed to AD following a 36-month follow-up. Ages of the individuals ranged from 55 to 90, and their MMSE scores for each group were 20 to 26 (AD), 24 to 30, and 24 to 30 (MCI).the ARWIBO data set from https://www.gaaindata.org and the NACC data collection from https://www.alz.washington.edu, all of which are freely accessible online. We employed a total of 694 structural MRI scans for this study, which were first

ISSN: 1992-8645 www.jatit.org E-ISSN: 1817-3195

divided into four categories: AD (n = 122) HCI (n = 130), EMCI (n = 69), and LMCI (n = 54).

4.2 Confusion matrix and evaluation metrics

An evaluation tool called a confusion matrix (CM) is used in statistics and machine learning to rate the precision of a classification model. The CM shows the number of times the test samples are classified correctly and incorrectly, relative to the true class labels. The confusion matrix is a 2×2 table showing four possible outcomes of the classification: The evaluation metrics are defined in Eqn(8)

$$\Pr = \frac{TP}{TP + FP}$$
$$Sp = \frac{TN}{TN + FP} \quad (8)$$
$$Acc = \frac{TP + TN}{TP + FP + TN + FN}$$
$$F1 = 2.\frac{Se.\Pr}{Se + \Pr}$$

- TP: The model correctly classified the positive samples.
- FN: The model incorrectly classified the positive samples.
- FP: The model incorrectly classified the negative samples.
- TN: The model correctly classified the negative samples.

This study selected different convolutional neural network-based models for training and testing in three different datasets. The experimental results of the proposed method using the ADNI dataset is given in Table 1 and the NACC dataset is given in Table 2.

Table 1: Detailed Results of the proposed DIAN-Net model with different Categories on the ADNI Data set

Methods	Accuracy	AUC	Sensitivity	Specificity	F1-Score
AD	0.91	0.91	0.90	0.90	**0.91**
NCI	0.92	0.91	0.90	0.91	**0.92**
sMCI	0.63	0.71	0.69	0.62	**0.63**
pMCI	0.93	0.93	0.93	0.92	**0.93**

The classification accuracy of the proposed method on AD class is 91%, NCI is 92%,sMCI class is 63% and pMCI class is 92%. Compared to the other classes our proposed model produces more than 90% except for sMCI classes. Experimental Results of the proposed model using cross-validation method on the ADNI Data set is given in Table 3.

Table 2: Detailed Results of the proposed DIAN-Net model with different Categories on the NACC and ARWIBO Data set

Methods	Accuracy	AUC	Sensitivity	Specificity	F1-Score
AD	0.91	0.91	0.90	0.90	0.91
NCI	0.89	0.90	0.86	0.87	0.89
sMCI	0.88	0.87	0.86	0.86	0.88
pMCI	0.94	0.94	0.94	0.94	0.94

The classification accuracy of the proposed method on AD class is 91%, NCI is 89%,sMCI class is 88% and pMCI class is 94%. Compared to the other classes our proposed model produces the best classification accuracy on pMCI classes.

Table 3: Experimental Results of DIAN-Net using the cross-validation method on the ADNI Data set

Images	Filter	Accuracy	Sensitivity	Specificity	F1 Score
ADNI Dataset	UNet++	0.93	0.93	0.92	0.93
	NASNet	0.93	0.94	0.92	0.93
	Inception-v3	0.92	0.93	0.90	0.91
	DenseNet	0.92	0.92	0.90	0.91
	ResNet50	0.92	0.92	0.90	0.91
	VGG16	0.92	0.92	0.90	0.91
	DIAN-Net	**0.95**	**0.94**	**0.94**	**0.94**

ISSN: 1992-8645 www.jatit.org E-ISSN: 1817-3195

5 . CONCLUSION

Machine learning technology has shown promising performance in AD incidence prediction with large-scale administrative health data. In this work, we will introduce the Dense Inception Attention Network (DIAN-Net), it is a combination of the Dense module, skin connection, triple attention block, and the Inception attention module. The proposed network consists of major three parts: the base encoder-decoder framework, an improved Dense module, and an inception attention module. Conventional dual-convolution structure in U-Net has limited feature representation ability. In addition, due to the limited receptive field, there are still some shortcomings in multi-level context representation to affect the whole segmentation performance. In our Inception Attention module, various types of convolution kernels are put at the bottom of the model. These convolution kernels have different receptive fields and can extract features of different scales, and the transformation through convolution does not change the size of the original image. The proposed DIAN-Net-based AD diagnosis method is validated using k-fold cross-validation method. The experimental results show that the algorithm in this paper has a smaller number of parameters and shorter training time, and outperforms other methods in terms of subjective visualization and objective evaluation metrics on multiple benchmark datasets.

REFERENCES

[1]. Kruthika, K., Maheshappa, H., Initiative, A.D.N., et al., 2019. Cbir system using capsule networks and 3d cnn for alzheimer's disease diagnosis. Informatics in Medicine Unlocked 14, 59–68.

[2]. Li, W., Lin, X., Chen, X., 2020. Detecting alzheimer's disease based on 4d fmri: An exploration under deep learning framework. Neurocomputing 388, 280–287.

[3].Liu, C., Huang, F., Qiu, A., Initiative, A.D.N., et al., 2023. Monte carlo ensemble neural network for the diagnosis of alzheimer's disease. Neural Networks 159, 14–24.

[4]. Nozadi S. H., Kadoury S. Classification of Alzheimer's and MCI patients from semantically parcelled PET images: a comparison between AV45 and FDG-PET. International Journal of Biomedical Imaging. 2018;2018:13.

[5]. Tatulian, S.A. Challenges and hopes for Alzheimer's disease. Drug Discov. Today **2022**, 27, 1027–1043.

[6]. Brookmeyer, R.; Johnson, E.; Ziegler-Graham, K.; Arrighi, H.M. Forecasting the global burden of Alzheimer's disease. Alzheimer's Dement. 2007, 3, 186–191.

[7].Yang X, Li H, Li X (2022) Lightweight image super-resolution with feature cheap convolution and attention mechanism. Cluster Computing 25(6):3977–3992.

[8].Zhang Y, Tian Y, Kong Y, et al (2020) Residual dense network for image restoration. IEEE transactions on pattern analysis and machine intelligence 43(7):2480–2495.

[9].Hui Z, Wang X, Gao X (2018) Fast and accurate single image super-resolution via information distillation network. In: Proceedings of the IEEE conference on computer vision and pattern recognition, pp 723–731.

[10]. Park, S., Hong, C.H., Lee, D.g., Park, K., Shin, Initiative, A.D.N., et al., 2023. Prospectiveclassification of alzheimer's disease conversion from mild cognitive impairment. Neural Networks .

[11].Wang, C., Li, Y., Tsuboshita, Y., Sakurai, T., Goto, T., Yamaguchi, H., Yamashita, Y., Sekiguchi, A., Tachimori, H., Initiative, A.D.N., 2022. A high-generalizability machine learning framework for predicting the progression of alzheimer's disease using limited data. NPJ digital medicine 5, 43.

[12].Khojaste-Sarakhsi, M., Haghighi, S.S., Ghomi, S.F., Marchiori, E., 2022. Deep learning for alzheimer's disease diagnosis: A survey. Artificial Intelligence in Medicine , 102332.

[13].Loi, S.M.; Pijnenberg, Y.; Velakoulis, D. Recent research advances in young-onset dementia. Curr. Opin. Psychiatry 2023, 36, 126–133. [CrossRef] [PubMed]

[14]. Zhang, W.; Xu, C.; Sun, J.; Shen, H.-M.; Wang, J.; Yang, C. Impairment of the autophagy–lysosomal pathway in Alzheimer's diseases: Pathogenic mechanisms and therapeutic potential. Acta Pharm. Sin. B 2022, 12, 1019–1040. [CrossRef] [PubMed]

[15]. Boeve, B.F.; Boxer, A.L.; Kumfor, F.; Pijnenburg, Y.; Rohrer, J.D. Advances and controversies in frontotemporal dementia: Diagnosis, biomarkers, and therapeutic considerations. Lancet Neurol. 2022, 21, 258–272. [CrossRef]

[16]. Sügis, E.; Dauvillier, J.; Leontjeva, A.; Adler, P.; Hindie, V.; Moncion, T.; Collura, V.; Daudin, R.; Loe-Mie, Y.; Herault, Y.; et al. HENA, heterogeneous network-based data set for Alzheimer's disease. Sci. Data 2019, 6, 151. [CrossRef]

[17]. Jayachandran, A & Dhanasekaran, R, "Severity Analysis of Brain Tumor in MRI Images using Modified Multi-Texton Structure Descriptor and Kernel- SVM, The Arabian Journal of science and engineering October 2014, Volume 39, Issue 10, pp 7073-7086,(2014).

[18]. Tzeng, R.-C.; Yang, Y.-W.; Hsu, K.-C.; Chang, H.-T.; Chiu, P.-Y. Sum of boxes of the clinical dementia rating scale highly predicts conversion or reversion in predementia stages. Front. Aging Neurosci. 2022, 14, 1021792. [CrossRef] [PubMed]

[19]. Hughes, C.P.; Berg, L.; Danziger,W.L.; Coben, L.A.; Martin, R.L. A New Clinical Scale for the Staging of Dementia. Br. J. Psychiatry 1982, 140, 566–572. [CrossRef]

[20]. Titheradge, D.; Isaac, M.; Bremner, S.; Tabet, N. Cambridge Cognitive Examination and Hachinski Ischemic Score as predictors of MRI confirmed pathology in dementia: A cross-sectional study. Int. J. Clin. Pract. 2019, 74, e13446. [CrossRef] [PubMed]

[21]. Schmand, B.; Walstra, G.; Lindeboom, J.; Teunisse, S.; Jonker, C. Early detection of Alzheimer's disease using the Cambridge Cognitive Examination (CAMCOG). Psychol. Med. 2000, 30, 619–627. [CrossRef] [PubMed]

[22]. Rocha, A.; Bellaver, B.; Souza, D.G.; Schu, G.; Fontana, I.C.; Venturin, G.T.; Greggio, S.; Fontella, F.U.; Schiavenin, M.L.; Machado,L.S.; et al. Clozapine induces astrocyte-dependent FDG-PET hypometabolism. Eur. J. Nucl. Med. 2022, 49, 2251–2264. [CrossRef]

[23]. Oe, K.; Zeng, F.; Niikura, T.; Fukui, T.; Sawauchi, K.; Matsumoto, T.; Nogami, M.; Murakami, T.; Kuroda, R. Influence of Metal Implants on Quantitative Evaluation of Bone Single-Photon Emission Computed Tomography/Computed Tomography. J. Clin.Med. 2022, 11, 6732. [CrossRef]

[24]. Madetko-Alster, N.; Alster, P.; Migda, B.; Nieciecki, M.; Koziorowski, D.; Królicki, L. The Use of Cerebellar Hypoperfusion Assessment in the Differential Diagnosis of Multiple System Atrophy with Parkinsonism and Progressive Supranuclear Palsy- Parkinsonism Predominant. Diagnostics 2022, 12, 3022. [CrossRef]

[25]. Garriga, M.; Emila, M.; Mir, M.; Eal-Baradie, R.; Ehuertas, S.; Ecastejon, C.; Ecasas, L.; Badenes, D.; Gimenez, N.; Font, M.A.;et al. 123I-FP-CIT SPECT imaging in early diagnosis of dementia in patients with and without a vascular component. Front. Syst. Neurosci. 2015, 9, 99. [CrossRef]

[26]. Fortea, J.; Carmona-Iragui, M.; Benejam, B.; Fernández, S.; Videla, L.; Barroeta, I.; Alcolea, D.; Pegueroles, J.; Muñoz, L.; Belbin, O.; et al. Plasma and CSF biomarkers for the diagnosis of Alzheimer's disease in adults with Down syndrome: A cross-sectional study. Lancet Neurol. **2018**, 17, 860–869.

[27].Shahid, S.S.;Wen, Q.; Risacher, S.L.; Farlow, M.R.; Unverzagt, F.W.; Apostolova, L.G.; Foroud, T.M.; Zetterberg, H.; Blennow, K.; Saykina, A.J.; et al. Hippocampal-subfield microstructures and their relation to plasma biomarkers in Alzheimer's disease. Brain 2022, 145, 2149–2160. [CrossRef]

[28]. Vaghari, D.; Kabir, E.; Henson, R.N. Late combination shows that MEG adds toMRI in classifying MCI versus controls. Neuroimage 2022, 252, 119054.

[29].Jesu Prabhu A and Jayachandran, A, "Mixture Model Segmentation System for Parasagittal Meningioma Brain Tumor Classification based on Hybrid Feature Vector" Journal of Medical System, vol 42, issues 12, 2018.

[30]. Jayachandran, A and R.Dhanasekaran ,(2017) 'Multi Class Brain Tumor Classification of MRI Images using Hybrid Structure Descriptor and Fuzzy Logic Based RBF Kernel SVM' , Iranian Journal of Fuzzy system , Volume 14, Issue 3, pp 41-54 , 2017.

[31].. Guévremont, D.; Tsui, H.; Knight, R.; Fowler, C.J.; Masters, C.L.; Martins, R.N.; Abraham, W.C.; Tate, W.P.; Cutfield, N.;

Williams, J.M. Plasma microRNA vary in association with the progression of Alzheimer's disease. Alzheimer's Dement. **2022**, 14, e12251.

[32]. Jayachandran, A, 'Abnormality segmentation and Classification of multi model brain tumor in MR images using Fuzzy based hybrid kernel SVM' International Journal of Fuzzy system , published by Springer, Volume 17, Issue 3, pp 434-443,2018.

[33].. Janousova, E.; Vounou, M.; Wolz, R.; Gray, K.R.; Rueckert, D.; Montana, G. Biomarker discovery for sparse classification of brain images in Alzheimer's disease. Ann. BMVA 2012, 2, 1–11.

[34]. Sonoda, S.; Murata, N. Neural network with unbounded activation functions is universal approximator. Appl. Comput. Harmon. Anal. 2017, 43, 233–268.

[35].Theckedath, D. and R.J.S.C.S. Sedamkar, Detecting affect states using VGG16, ResNet50 and SE-ResNet50 networks. 2020. 1: p. 1-7.

[36]. Mahiba C, A Jayachandran,"Severity analysis of diabetic retinopathy in retinal images using hybrid structure descriptor and modified CNNs",Measurement,Vol 135,PP 762-767,2019.

[37].Huang, G., Liu, Z., Van Der Maaten, L., Weinberger, K.Q.: Densely connected convolutional networks. In: 2017 IEEE Conference on Computer Vision and Pattern Recognition (CVPR), pp. 2261{2269 (2017).

[38].Zoph, B., Vasudevan, V., Shlens, J., Le, Q.V.: Learning transferable architectures for scalable image recognition. In: 2018 IEEE/CVF Conference on Computer Vision and Pattern Recognition, pp. 8697{8710 (2018).

[39].Tulsani A, P. Kumar, S. Pathan, Automated segmentation of optic disc and optic cup for glaucoma assessment using improved unet++ architecture, Biocybern Biomed Eng 41 (18),2021.